Available online at www.sciencedirect.com
SCIENCE DIRECT
Journal of Sound and Vibration 297 (2006) 89–105
JOURNAL OF SOUND AND VIBRATION
www.elsevier.com/locate/jsvi

Dual reciprocity boundary element method solution of the Cauchy problem for Helmholtz-type equations with variable coefficients

L. Marin[a,*], L. Elliott[b], P.J. Heggs[c], D.B. Ingham[b], D. Lesnic[b], X. Wen[a]

[a]School of Earth and Environment, University of Leeds, Leeds LS2 9JT, UK
[b]Department of Applied Mathematics, University of Leeds, Leeds LS2 9JT, UK
[c]School of Chemical Engineering and Analytical Science, University of Manchester, Sackville Street, P.O. Box 88, Manchester M60 1QD, UK

Received 22 November 2004; received in revised form 16 January 2006; accepted 16 March 2006
Available online 6 June 2006

Abstract

In this paper, the application of the dual reciprocity boundary element method (DRBEM) to the Cauchy problem for Helmholtz-type equations with variable coefficients is investigated. The resulting system of linear algebraic equations is ill-conditioned and therefore its solution is regularized by employing the zeroth-order Tikhonov functional, while the choice of the regularization parameter is based on the L-curve method. Numerical results are presented for Cauchy problems in smooth and piecewise smooth geometries, as well as simply and doubly connected domains. The accuracy, convergence and stability of the proposed numerical method with respect to various approximating functions, various DRBEM discretizations and various levels of noise added in the boundary data, respectively, are also analysed.

1. Introduction

The Helmholtz equation arises naturally in many physical applications related to wave propagation and vibration phenomena. It is often used to describe the vibration of a structure [1], the acoustic cavity problem [2], the radiation wave [3] and the scattering of a wave [4]. Another important application of the Helmholtz equation is the problem of heat conduction in fins [5–7]. The knowledge of the Dirichlet, Neumann or mixed boundary conditions on the entire boundary of the solution domain gives rise to direct problems for Helmholtz-type equations which have been extensively studied in the literature, see for example Refs. [8–10]. The well-posedness of the direct problems for the Helmholtz equation by the removal of the eigenvalues of the Laplacian operator is well established, see e.g. Ref. [11].

In many engineering problems the boundary conditions are often incomplete, either in the form of under-specified and over-specified boundary conditions on different parts of the boundary or the solution is

*Corresponding author. School of Mechanical, Materials and Manufacturing Engineering, The University of Nottingham, University Park, Nottingham NG7 2RD, UK. Tel.: +44 115 846 7683; fax: +44 115 951 3800.
E-mail address: liviu.marin@nottingham.ac.uk (L. Marin).

0022-460X/$ - see front matter © 2006 Elsevier Ltd. All rights reserved.
doi:10.1016/j.jsv.2006.03.045

prescribed at some internal points in the domain. These are *inverse problems* and it is well known that they are generally ill-posed, i.e. the existence, uniqueness and stability of their solutions are not always guaranteed, see e.g. Ref. [12]. A classical example of an inverse problem for Helmholtz-type equations is the Cauchy problem in which boundary conditions for both the solution and its normal derivative are prescribed only on a part of the boundary of the solution domain, whilst no information is available on the remaining part of the boundary. Unlike in direct problems, the uniqueness of the Cauchy problem is guaranteed without the necessity of removing the eigenvalues for the Laplacian. However, the Cauchy problem suffers from the global non-existence and instability of the solution.

A boundary element method (BEM)-based acoustic holography technique using the singular value decomposition (SVD) for the reconstruction of sound fields generated by irregularly shaped sources has been developed by Bai [13]. The vibrational velocity, sound pressure and acoustic power on the vibrating boundary comprising an enclosed space have been reconstructed by Kim and Ih [14] who have used the SVD in order to obtain the inverse solution in the least-squares sense and to express the acoustic modal expansion between the measurement and source field. Wang and Wu [15] have developed a method employing the spherical wave expansion theory and a least-squares minimization to reconstruct the acoustic pressure field from a vibrating object and their method has been extended to the reconstruction of acoustic pressure fields inside the cavity of a vibrating object by Wu and Yu [16]. DeLillo et al. [17] have detected the source of acoustical noise inside the cabin of a midsize aircraft from measurements of the acoustical pressure field inside the cabin by solving a linear Fredholm integral equation of the first kind in two-dimensions and they have extended this study to three-dimensional problems, see Ref. [18]. Marin et al. [19,20] have solved the Cauchy problem associated to the Helmholtz equation using the BEM in conjunction with an alternating iterative procedure consisting of obtaining successive solutions to well-posed mixed boundary value problems and with the conjugate gradient method (CGM), respectively. Recently, these methods have been compared with the Tikhonov regularization method and SVD by Marin et al. [21], whilst the same authors have proposed an iterative algorithm based on the Landweber method in combination with the BEM [22].

To our knowledge, the Cauchy problem associated with Helmholtz-type equations with variable coefficients has not been investigated as yet. In this paper, we present and analyse a numerical technique based on the dual reciprocity BEM (DRBEM), in conjunction with the Tikhonov regularization method, in order to solve the Cauchy problem for Helmholtz-type equations with spacewise dependent coefficients in open bounded domains, i.e. interior domains of finite size. The problem is regularized by choosing the optimal regularization parameter according to the L-curve criterion, see e.g. Ref. [23]. Four examples associated with smooth and piecewise smooth geometries, as well as simply and doubly connected domains, are presented. In addition, the accuracy, convergence and stability of the proposed numerical method with respect to various approximating functions, various DRBEM meshes and various levels of noise added in the input boundary data, respectively, are also analysed.

2. Mathematical formulation

Consider an open bounded domain $\Omega \subset \mathbb{R}^2$, i.e. interior domain of finite size, and assume that Ω is bounded by a piecewise smooth boundary $\Gamma \equiv \partial\Omega$, such that $\Gamma = \Gamma_1 \cup \Gamma_2$, where $\Gamma_1, \Gamma_2 \neq \emptyset$ and $\Gamma_1 \cap \Gamma_2 = \emptyset$. Referring to acoustics for the sake of the physical explanation, we assume that the acoustical field $u(\mathbf{x})$ satisfies the Helmholtz-type equation in the domain Ω, namely

$$\mathscr{L}(\mathbf{x}, u(\mathbf{x})) \equiv (\Delta \pm k(\mathbf{x}))u(\mathbf{x}) = b_0(\mathbf{x}), \quad \mathbf{x} \in \Omega, \tag{1}$$

where $k(\mathbf{x}) > 0$, $\mathbf{x} \in \overline{\Omega}$, is the spacewise dependent frequency of the acoustical field u and $b_0(\mathbf{x})$, $\mathbf{x} \in \Omega$, is the source term. Let $\mathbf{n}(\mathbf{x})$ be the outward unit normal vector at Γ and $\phi(\mathbf{x}) \equiv (\nabla u \cdot \mathbf{n})(\mathbf{x})$ be the normal velocity of the sound at a point $\mathbf{x} \in \Gamma$. In the direct problem formulation, the knowledge of the acoustical field and/or normal velocity of the sound on the whole boundary Γ gives the corresponding Dirichlet, Neumann, or mixed boundary conditions which enables us to determine the acoustical field in the domain Ω. If it is possible to measure both the acoustical field and the normal velocity of the sound on a part of the boundary Γ, say Γ_1, then this leads to the mathematical formulation of an inverse problem consisting of Eq. (1) and the

boundary conditions

$$u(\mathbf{x}) = \widetilde{u}(\mathbf{x}), \quad \phi(\mathbf{x}) = \widetilde{\phi}(\mathbf{x}), \quad \mathbf{x} \in \Gamma_1, \tag{2}$$

where $\widetilde{u}$ and $\widetilde{\Phi}$ are prescribed functions and $\Gamma_1 \subset \Gamma$, meas$(\Gamma_1) > 0$. In the above formulation of the boundary conditions (2), it can be seen that the boundary Γ_1 is over-specified by prescribing both the acoustical field $u|_{\Gamma_1}$ and the normal velocity of the sound $\phi|_{\Gamma_1}$, whilst the boundary $\Gamma_2 = \Gamma \backslash \Gamma_1$ is under-specified since both the acoustical field $u|_{\Gamma_2}$ and the normal velocity of the sound $\phi|_{\Gamma_2}$ are unknown and have to be determined.

This problem, termed the Cauchy problem, is much more difficult to solve both analytically and numerically than the direct problem, since the solution does not satisfy the general conditions of well-posedness. Whilst the Dirichlet, Neumann or mixed direct problems associated to Eq. (1) do not always have a unique solution due to the eigensolutions, see Ref. [11], the solution of the Cauchy problem given by Eqs. (1) and (2) is unique based on the analytical continuation property. However, it is well known that if this solution exists then it is unstable with respect to small perturbations in the data on Γ_2, see e.g. Ref. [12]. Thus the problem under investigation is ill-posed and we cannot use a direct approach, such as the Gauss elimination method, in order to solve the system of linear equations which arises from the discretization of the partial differential equations (1) and thee boundary conditions (2). Therefore, regularization methods are required in order to solve accurately the Cauchy problem associated with Helmholtz-type equations with variable coefficients.

3. Dual reciprocity boundary element method

The DRBEM, which was originally introduced by Nardini and Brebbia [24], has become a widely used method for solving inhomogeneous and nonlinear boundary value problems for partial differential equations as an extension of the BEM. The main idea of this method consists of employing the fundamental solution corresponding to a simpler equation and considering the remaining terms of the original equation via a procedure which involves a series expansion using global approximating functions and the reciprocity principles. For the sake of completeness, in this section we describe the DRBEM applied to Helmholtz-type equations. For further details of the DRBEM, we refer the reader to Ref. [25].

In the view of the DRBEM, the Helmholtz-type equation (1) is rewritten as

$$\Delta u(\mathbf{x}) = b(\mathbf{x}, u(\mathbf{x})), \quad \mathbf{x} \in \Omega, \tag{3}$$

where

$$b(\mathbf{x}, u(\mathbf{x})) = b_0(\mathbf{x}) \mp k(\mathbf{x})u(\mathbf{x}). \tag{4}$$

As a consequence, the left-hand side of Eq. (3) is dealt with by employing the fundamental solution for the Laplace equation, whilst the integrals corresponding to the right-hand side, $b(\mathbf{x}, u(\mathbf{x}))$, are taken to the boundary using the following approximation:

$$b(\mathbf{x}, u(\mathbf{x})) \approx \sum_{j=1}^{N+L} \alpha_j f_j(\mathbf{x}), \quad \mathbf{x} \in \Omega, \tag{5}$$

where α_j, $j = 1, \ldots, (N+L)$, are initially unknown coefficients and $f_j(\mathbf{x})$, $j = 1, \ldots, (N+L)$, are specified approximating functions. The approximation is performed at N boundary nodes, $\mathbf{x}^i$, $i = 1, \ldots, N$, and L internal nodes, $\mathbf{x}^i$, $i = (N+1), \ldots, (N+L)$, which are called the DRBEM collocation nodes. The approximating functions used in this study are the so-called radial basis functions (RBFs), $f_j(\mathbf{x}) \equiv f_j(r) = 1 + r + \cdots + r^{2k-1}$, $k = 1, 2, 3$, and the thin plate spline (TPS), $f_j(\mathbf{x}) \equiv f_j(r) = r^2 \ln r$, where r is the distance function used in the definition of the fundamental solution. The DRBEM employs a series of particular solutions, $\widehat{u}_j$, $j = 1, \ldots, (N+L)$, which are related to the approximating functions, f_j, $j = 1, \ldots, (N+L)$, through the following expression:

$$\Delta \widehat{u}_j(\mathbf{x}) = f_j(\mathbf{x}), \quad j = 1, \ldots, (N+L), \quad \mathbf{x} \in \Omega. \tag{6}$$

On substituting Eq. (6) into relation (5), we obtain the following approximation for the original right-hand side of the Helmholtz-type equation (3):

$$b(\mathbf{x}, u(\mathbf{x})) \approx \sum_{j=1}^{N+L} \alpha_j \, \Delta \widehat{u}_j(\mathbf{x}), \quad \mathbf{x} \in \Omega. \tag{7}$$

Next, the standard BEM procedure is applied. More precisely, Eq. (7) is multiplied by the fundamental solution for the Laplace equation, namely

$$u^*(\mathbf{x}, \mathbf{y}) = -\frac{1}{2\pi} \ln r(\mathbf{x}, \mathbf{y}) \tag{8}$$

and integrated over the domain Ω:

$$\int_\Omega u^*(\mathbf{x}, \mathbf{y}) \, \Delta u(\mathbf{y}) \, \mathrm{d}\Omega(\mathbf{y}) = \sum_{j=1}^{N+L} \alpha_j \int_\Omega u^*(\mathbf{x}, \mathbf{y}) \, \Delta \widehat{u}_j(\mathbf{y}) \, \mathrm{d}\Omega(\mathbf{y}), \quad \mathbf{x} \in \overline{\Omega}. \tag{9}$$

By applying Green's formula to Eq. (9), the boundary integral equation is obtained as

$$\begin{aligned} & c(\mathbf{x}) u(\mathbf{x}) + \int_\Gamma \phi^*(\mathbf{x}, \mathbf{y}) \, u(\mathbf{y}) \, \mathrm{d}\Gamma(\mathbf{y}) - \int_\Gamma u^*(\mathbf{x}, \mathbf{y}) \, \phi(\mathbf{y}) \, \mathrm{d}\Gamma(\mathbf{y}) \\ & = \sum_{j=1}^{N+L} \alpha_j \left(c(\mathbf{x}) \widehat{u}_j(\mathbf{x}) + \int_\Gamma \phi^*(\mathbf{x}, \mathbf{y}) \, \widehat{u}_j(\mathbf{y}) \, \Gamma(\mathbf{y}) - \int_\Gamma u^*(\mathbf{x}, \mathbf{y}) \, \widehat{\phi}_j(\mathbf{y}) \, \mathrm{d}\Gamma(\mathbf{y}) \right), \quad \mathbf{x} \in \overline{\Omega}, \end{aligned} \tag{10}$$

where $\phi^*(\mathbf{x}, \mathbf{y}) \equiv \nabla u^*(\mathbf{x}, \mathbf{y}) \cdot \mathbf{n}(\mathbf{y})$, $\phi(\mathbf{y}) \equiv (\nabla u \cdot \mathbf{n})(\mathbf{y})$ and $\widehat{\phi}_j(\mathbf{y}) \equiv (\nabla \widehat{u}_j \cdot \mathbf{n})(\mathbf{y})$, $j = 1, \ldots, (N + L)$, for $\mathbf{x} \in \overline{\Omega}$ and $\mathbf{y} \in \Gamma$, while $c(\mathbf{x}) = 1$ for $\mathbf{x} \in \Omega$ and $c(\mathbf{x}) = 0.5$ for $\mathbf{x} \in \Gamma$ smooth.

A BEM with piecewise constant boundary elements is used in order to discretize the boundary integral equation (10). Consequently, the boundary Γ of the solution domain Ω is approximated by N straight line segments, Γ_k, $k = 1, \ldots, N$, in a counterclockwise sense, whilst the acoustical field, u, the normal velocity of the sound, ϕ, the particular solutions, $\widehat{u}_j$, $j = 1, \ldots, (N + L)$, and its normal derivative, $\widehat{\phi}_j$, $j = 1, \ldots, (N + L)$, are considered to be constant and take their values at the midpoint, $\mathbf{x}^k \in \Gamma_k$, $k = 1, \ldots, N$, i.e. collocation point, also known as the node, of each element. Hence the discretized boundary integral equation may be recast as

$$\begin{aligned} & c(\mathbf{x}) u(\mathbf{x}) + \sum_{k=1}^{N} \left(\int_{\Gamma_k} \phi^*(\mathbf{x}, \mathbf{y}) \, \mathrm{d}\Gamma(\mathbf{y}) \right) u(\mathbf{x}^k) - \sum_{k=1}^{N} \left(\int_{\Gamma_k} u^*(\mathbf{x}, \mathbf{y}) \, \mathrm{d}\Gamma(\mathbf{y}) \right) \phi(\mathbf{x}^k) \\ & = \sum_{j=1}^{N+L} \alpha_j \left\{ c(\mathbf{x}) \widehat{u}_j(\mathbf{x}) + \sum_{k=1}^{N} \left(\int_{\Gamma_k} \phi^*(\mathbf{x}, \mathbf{y}) \, \mathrm{d}\Gamma(\mathbf{y}) \right) \widehat{u}_j(\mathbf{x}^k) - \sum_{k=1}^{N} \left(\int_{\Gamma_k} u^*(\mathbf{x}, \mathbf{y}) \, \mathrm{d}\Gamma(\mathbf{y}) \right) \widehat{\phi}_j(\mathbf{x}^k) \right\}, \\ & \mathbf{x} \in \overline{\Omega}. \end{aligned} \tag{11}$$

By applying the discretized boundary integral equation (11) at each boundary and internal collocation point $\mathbf{x}^i$, $i = 1, \ldots, (N + L)$, we arrive at the DRBEM system of linear algebraic equations

$$\mathbf{H}\mathbf{u} - \mathbf{G}\boldsymbol{\phi} = \left(\mathbf{H}\widehat{\mathbf{U}} - \mathbf{G}\widehat{\boldsymbol{\Phi}} \right) \boldsymbol{\alpha}, \tag{12}$$

where $\mathbf{H}, \mathbf{G} \in \mathbb{R}^{(N+L)\times(N+L)}$ are the BEM matrices corresponding to the Laplace equation, $\widehat{\mathbf{U}}, \widehat{\boldsymbol{\Phi}} \in \mathbb{R}^{(N+L)\times(N+L)}$ are the DRBEM matrices, $\mathbf{u}, \boldsymbol{\phi} \in \mathbb{R}^{N+L}$ are vectors containing the values of the acoustical field and the normal velocity of the sound, respectively, at the collocation points and $\boldsymbol{\alpha} \in \mathbb{R}^{N+L}$ is a vector containing the unknowns α_j, $j = 1, \ldots, (N + L)$. More specifically, the components of the above matrices and vectors are given by

$$H_{ik} = \begin{cases} \frac{1}{2}\delta_{ik} + \int_{\Gamma_k} \phi^*(\mathbf{x}^i, \mathbf{y}) \, \mathrm{d}\Gamma(\mathbf{y}), & 1 \leqslant i \leqslant N, \;\; 1 \leqslant k \leqslant N, \\ 0, & 1 \leqslant i \leqslant N, \;\; N+1 \leqslant k \leqslant N+L, \\ \int_{\Gamma_k} \phi^*(\mathbf{x}^i, \mathbf{y}) \, \mathrm{d}\Gamma(\mathbf{y}), & N+1 \leqslant i \leqslant N+L, \;\; 1 \leqslant k \leqslant N, \\ \delta_{ik}, & N+1 \leqslant i \leqslant N+L, \;\; N+1 \leqslant k \leqslant N+L, \end{cases} \tag{13}$$

$$G_{ik} = \begin{cases} \int_{\Gamma_k} u^*(\mathbf{x}^i, \mathbf{y})\, \mathrm{d}\Gamma(\mathbf{y}), & 1 \leqslant i \leqslant N, \quad 1 \leqslant k \leqslant N, \\ 0, & 1 \leqslant i \leqslant N, \quad N+1 \leqslant k \leqslant N+L, \\ \int_{\Gamma_k} u^*(\mathbf{x}^i, \mathbf{y})\, \mathrm{d}\Gamma(\mathbf{y}), & N+1 \leqslant i \leqslant N+L, \quad 1 \leqslant k \leqslant N, \\ 0, & N+1 \leqslant i \leqslant N+L, \quad N+1 \leqslant k \leqslant N+L, \end{cases} \tag{14}$$

$$\widehat{U}_{kj} = \widehat{u}_j(\mathbf{x}^k) = \widehat{u}(r(\mathbf{x}^k, \mathbf{x}^j)), \quad 1 \leqslant k \leqslant N+L, \quad 1 \leqslant j \leqslant N+L, \tag{15}$$

$$\widehat{\Phi}_{kj} = \begin{cases} \widehat{\phi}_j(\mathbf{x}^k) = \widehat{\phi}(r(\mathbf{x}^k, \mathbf{x}^j)), & 1 \leqslant k \leqslant N, \quad 1 \leqslant j \leqslant N+L, \\ 0, & N+1 \leqslant k \leqslant N+L, \quad 1 \leqslant j \leqslant N+L, \end{cases} \tag{16}$$

$$\begin{aligned} &u_k = u(\mathbf{x}^k), \quad \phi_k = \phi(\mathbf{x}^k), \quad 1 \leqslant k \leqslant N, \\ &u_k = u(\mathbf{x}^k), \quad \phi_k = 0, \quad N+1 \leqslant k \leqslant N+L. \end{aligned} \tag{17}$$

The vector $\boldsymbol{\alpha} \in \mathbb{R}^{N+L}$ in Eq. (12) can be calculated by collocating Eq. (5) at the DRBEM collocation points $\mathbf{x}^i$, $i = 1, \ldots, (N+L)$, i.e.

$$\boldsymbol{\alpha} = \widetilde{\mathbf{F}}^{-1}\mathbf{b}. \tag{18}$$

Here components of the matrix $\widetilde{\mathbf{F}} \in \mathbb{R}^{(N+L)\times(N+L)}$ are given by

$$\widetilde{F}_{ij} = f_j(\mathbf{x}^i) = f(r(\mathbf{x}^j, \mathbf{x}^i)), \quad 1 \leqslant i, j \leqslant N+L, \tag{19}$$

whilst, in the case of Helmholtz-type equations the components of the vector $\mathbf{b} \in \mathbb{R}^{N+L}$ are calculated as

$$b_i = b_0(\mathbf{x}^i) \mp k(\mathbf{x}^i) u(\mathbf{x}^i), \quad 1 \leqslant i \leqslant N+L, \tag{20}$$

or in matrix form as

$$\mathbf{b} = \mathbf{b}_0 + \mathbf{K}\mathbf{u}, \quad b_{0j} = b_0(\mathbf{x}^j), \quad K_{ij} = \mp\delta_{ij}\, k(\mathbf{x}^j), \quad 1 \leqslant i, j \leqslant N+L. \tag{21}$$

On substituting Eq. (21) into Eq. (18), we obtain

$$\boldsymbol{\alpha} = \widetilde{\mathbf{F}}^{-1}(\mathbf{b}_0 + \mathbf{K}\mathbf{u}) \tag{22}$$

and hence the DRBEM system of linear algebraic equations (12) associated with the Helmholtz-type equation (1) may be recast as

$$\overline{\mathbf{H}}\mathbf{u} - \mathbf{G}\boldsymbol{\phi} = \mathbf{d}, \tag{23}$$

where

$$\overline{\mathbf{H}} = \mathbf{H} - \mathbf{S}\mathbf{K}, \quad \mathbf{S} = (\mathbf{H}\widehat{\mathbf{U}} - \mathbf{G}\widehat{\boldsymbol{\Phi}})\widetilde{\mathbf{F}}^{-1}, \quad \mathbf{d} = \mathbf{S}\mathbf{b}_0. \tag{24}$$

4. Regularization

If the boundaries Γ_1 and Γ_2 of the solution domain Ω are discretized into N_1 and N_2 boundary elements, respectively, such that $N_1 + N_2 = N$ then the DRBEM system of linear algebraic equations (23) associated with the Helmholtz-type equation (1) may be recast as a system of $(N+L)$ linear algebraic equations with $(2N_2 + L)$ unknowns which can be generically written as

$$\mathbf{C}\mathbf{X} = \mathbf{F}, \tag{25}$$

where the system matrix $\mathbf{C} \in \mathbb{R}^{(N+L)\times(2N_2+L)}$, the unknown vector $\mathbf{X} \in \mathbb{R}^{2N_2+L}$ and the right-hand side vector $\mathbf{F} \in \mathbb{R}^{N+L}$ are given by

$$\begin{cases} C_{ij-N_1} = -G_{ij}, & 1 \leqslant i \leqslant N+L, \quad N_1+1 \leqslant j \leqslant N, \\ C_{ij+N_2-N_1} = S_{ij}, & 1 \leqslant i \leqslant N+L, \quad N_1+1 \leqslant j \leqslant N+L, \end{cases} \tag{26}$$

$$\begin{cases} X_{j-N_1} = \phi_j, & N_1+1 \leqslant j \leqslant N, \\ X_{j+N_2-N_1} = u_j, & N_1+1 \leqslant j \leqslant N+L, \end{cases} \tag{27}$$

$$F_i = \sum_{j=1}^{N_1} (-S_{ij}\widetilde{\phi}_j + G_{ij}\widetilde{u}_j), \quad 1 \leqslant i \leqslant N+L, \tag{28}$$

where

$$\widetilde{\phi}_j = \widetilde{\phi}(\mathbf{x}^j), \quad \widetilde{u}_j = \widetilde{u}(\mathbf{x}^j), \quad 1 \leqslant j \leqslant N_1. \tag{29}$$

4.1. Tikhonov regularization method

It should be noted that the system of linear algebraic equations (25) is ill-conditioned and cannot be solved by direct methods, such as the least-squares method, since such an approach would produce a highly unstable solution due to the large value of the condition number of the matrix $\mathbf{C}$ which increases dramatically as the number of DRBEM collocation points increases. Several regularization procedures have been developed to solve such ill-conditioned systems, see for example Ref. [23]. However, we only consider the Tikhonov regularization method, see Ref. [26], in our study since it is simple, non-iterative and it provides an explicit solution, see Eq. (33) below. Furthermore, the Tikhonov regularization method is feasible to apply for large systems of equations unlike the SVD which may become prohibitive for such large problems, see Ref. [27].

The Tikhonov regularized solution to the system of linear algebraic equations (25) is sought as

$$\mathbf{X}_\lambda : \mathscr{T}_\lambda(\mathbf{X}_\lambda) = \min_{\mathbf{X} \in \mathbb{R}^{2N_2+L}} \mathscr{T}_\lambda(\mathbf{X}), \tag{30}$$

where $\mathscr{T}_\lambda$ represents the sth order Tikhonov functional given by

$$\mathscr{T}_\lambda(\cdot) : \mathbb{R}^{2N_2+L} \longrightarrow [0, \infty), \quad \mathscr{T}_\lambda(\mathbf{X}) = \|\mathbf{C}\mathbf{X} - \mathbf{F}\|_2^2 + \lambda \|\mathbf{R}^{(s)}\mathbf{X}\|_2^2, \tag{31}$$

the matrix $\mathbf{R}^{(s)} \in \mathbb{R}^{(2N_2+L-s)\times(2N_2+L)}$ induces a $\mathscr{C}^s$-constraint on the solution $\mathbf{X}$ and $\lambda > 0$ is the regularization parameter to be chosen. For example, in the case of the zeroth-, first- and second-order Tikhonov regularization method the matrix $\mathbf{R}^{(s)}$, i.e. $s = 0, 1, 2$, is given by, see e.g. Ref. [28]:

$$\mathbf{R}^{(0)} = \begin{bmatrix} 1 & 0 & \dots & 0 \\ 0 & 1 & \dots & 0 \\ \vdots & \vdots & \ddots & \vdots \\ 0 & 0 & \dots & 1 \end{bmatrix} \in \mathbb{R}^{(2N_2+L)\times(2N_2+L)},$$

$$\mathbf{R}^{(1)} = \begin{bmatrix} -1 & 1 & 0 & \dots & 0 \\ 0 & -1 & 1 & \dots & 0 \\ \vdots & \vdots & \ddots & \ddots & \vdots \\ 0 & 0 & \dots & -1 & 1 \end{bmatrix} \in \mathbb{R}^{(2N_2+L-1)\times(2N_2+L)},$$

$$\mathbf{R}^{(2)} = \begin{bmatrix} 1 & -2 & 1 & 0 & \dots & 0 \\ 0 & 1 & -2 & 1 & \dots & 0 \\ \vdots & \vdots & \ddots & \ddots & \ddots & \vdots \\ 0 & 0 & \dots & 1 & -2 & 1 \end{bmatrix} \in \mathbb{R}^{(2N_2+L-2)\times(2N_2+L)}. \tag{32}$$

Formally, the Tikhonov regularized solution $\mathbf{X}_\lambda$ of the problem (30) is given as the solution of the regularized equation

$$(\mathbf{C}^{\mathrm{T}}\mathbf{C} + \lambda \mathbf{R}^{(s)^{\mathrm{T}}}\mathbf{R}^{(s)})\mathbf{X} = \mathbf{C}^{\mathrm{T}}\mathbf{F}. \tag{33}$$

Regularization is necessary when solving ill-conditioned systems of linear equations because the simple least-squares solution, i.e. $\lambda = 0$, is completely dominated by contributions from data errors and rounding errors. By adding regularization we are able to damp out these contributions and maintain the norm $\|\mathbf{R}^{(s)}\mathbf{X}\|_2$ to be of reasonable size.

4.2. Choice of the regularization parameter

The choice of the regularization parameter in Eq. (33) is crucial for obtaining a stable solution and this is discussed next. If too much regularization, or damping, i.e. $\lambda > 0$ is large, is imposed on the solution then it will not fit the given data $\mathbf{F}$ properly and the residual norm $\|\mathbf{CX} - \mathbf{F}\|_2$ will be too large. If too little regularization is imposed on the solution, i.e. $\lambda > 0$ is small, then the fit will be good, but the solution will be dominated by the contributions from the data errors, and hence $\|\mathbf{R}^{(s)}\mathbf{X}\|_2$ will be too large. It is quite natural to plot the norm of the solution as a function of the norm of the residual parametrized by the regularization parameter λ, i.e. $\{\|\mathbf{CX}_\lambda - \mathbf{F}\|_2, \|\mathbf{R}^{(s)}\mathbf{X}_\lambda\|_2, \lambda > 0\}$. Hence, the L-curve is really a trade-off curve between two quantities that both should be controlled and, according to the L-curve criterion, the optimal value λ_{opt} of the regularization parameter λ is chosen at the "corner" of the L-curve, see Ref. [23,27]. To summarize, the Tikhonov regularization method solves a minimization problem using different smoothness constraints, e.g. see expressions (32) for the matrix $\mathbf{R}^{(s)}$, in order to provide a stable solution which fits the data and also has a minimum structure.

As with every practical method, the L-curve has its advantages and disadvantages. There are two main disadvantages or limitations of the L-curve criterion. The first disadvantage is concerned with the reconstruction of very smooth exact solutions, see Ref. [29]. For such solutions, Hanke [30] showed that the L-curve criterion will fail, and the smoother the solution, the worse the regularization parameter λ computed by the L-curve criterion. However, it is not clear how often very smooth solutions arise in applications. The second limitation of the L-curve criterion is related to its asymptotic behaviour as the problem size $(2N_2 + L)$ increases. As pointed out by Vogel [31], the regularization parameter λ computed by the L-curve criterion may not behave consistently with the optimal parameter λ_{opt} as $(2N_2 + L)$ increases. However, this ideal situation in which the same problem is discretized for increasing $(2N_2 + L)$ may not arise so often in practice. Often the problem size $(2N_2 + L)$ is fixed by the particular measurement setup given by N and L, and if a larger $(2N_2 + L)$ is required then a new experiment must be undertaken. Apart from these two limitations, the advantages of the L-curve criterion are its robustness and ability to treat perturbations consisting of correlated noise, see for more details Ref. [27].

5. Numerical results and discussion

In this section, we illustrate the numerical results obtained using the DRBEM described in Section 3 combined with the zeroth-order Tikhonov regularization method, i.e. $s = 0$ in Eqs. (30) and (33), presented in Section 4 for solving the two-dimensional Cauchy problem given by Eqs. (1) and (2) corresponding to both the modified Helmholtz equation, i.e. $\mathscr{L}(\mathbf{x}, u(\mathbf{x})) \equiv (\Delta - k(\mathbf{x}))u(\mathbf{x})$, and the Helmholtz equation, i.e. $\mathscr{L}(\mathbf{x}, u(\mathbf{x})) \equiv (\Delta + k(\mathbf{x}))u(\mathbf{x})$, in smooth and piecewise smooth geometries, as well as simply and doubly connected domains.

5.1. Examples

In order to present the performance of the numerical method proposed, we consider the following analytical solutions for the acoustical field $u^{(\text{an})}(\mathbf{x})$ and the normal velocity of the sound $\phi^{(\text{an})}(\mathbf{x})$, as well as the corresponding values for the space-dependent coefficient $k(\mathbf{x})$ and the free term $b_0(\mathbf{x})$:

Example 1 (*Modified Helmholtz equation*).

$$\begin{aligned} &u^{(\mathrm{an})}(\mathbf{x}) = \exp(a_1 x_1^2 + a_2 x_2), && \mathbf{x} = (x_1, x_2) \in \Omega, \\ &\phi^{(\mathrm{an})}(\mathbf{x}) = -[2a_1 x_1 n_1(\mathbf{x}) + a_2 n_2(\mathbf{x})] \exp\left(a_1 x_1^2 + a_2 x_2\right), && \mathbf{x} = (x_1, x_2) \in \Gamma, \\ &k(\mathbf{x}) = 2a_1 + 4a_1^2 x_1^2 + a_2^2 > 0, && \mathbf{x} = (x_1, x_2) \in \overline{\Omega}, \\ &b_0(\mathbf{x}) = 0, && \mathbf{x} = (x_1, x_2) \in \Omega, \end{aligned} \tag{34}$$

where $a_1 = 1.0$ and $a_2 = -1.0$.

Example 2 (*Helmholtz equation*).

$$\begin{aligned} &u^{(\mathrm{an})}(\mathbf{x}) = \cos(a_1 x_1^2 + a_2 x_2), && \mathbf{x} = (x_1, x_2) \in \Omega, \\ &\phi^{(\mathrm{an})}(\mathbf{x}) = -[2a_1 x_1 n_1(\mathbf{x}) + a_2 n_2(\mathbf{x})] \sin\left(a_1 x_1^2 + a_2 x_2\right), && \mathbf{x} = (x_1, x_2) \in \Gamma, \\ &k(\mathbf{x}) = 4a_1^2 x_1^2 + a_2^2 > 0, && \mathbf{x} = (x_1, x_2) \in \overline{\Omega}, \\ &b_0(\mathbf{x}) = -2a_1 \sin\left(a_1 x_1^2 + a_2 x_2\right), && \mathbf{x} = (x_1, x_2) \in \Omega, \end{aligned} \tag{35}$$

where $a_1 = 1.0$ and $a_2 = 2.0$.

The examples defined by relations (34) and (35) are analysed in the following geometries:

Domain 1 (*Disk: Simply connected domain, smooth boundary*).

$$\begin{aligned} \Omega &= \{\mathbf{x} = (x_1, x_2) | x_1^2 + x_2^2 < R^2\}, \\ \Gamma &= \{\mathbf{x} = (x_1, x_2) | x_1^2 + x_2^2 = R^2\}, \\ \Gamma_1 &= \{\mathbf{x} = (x_1, x_2) \in \Gamma | 0 < \theta(\mathbf{x}) < 3\pi/2\}, \\ \Gamma_2 &= \{\mathbf{x} = (x_1, x_2) \in \Gamma | 3\pi/2 < \theta(\mathbf{x}) < 2\pi\}, \end{aligned} \tag{36}$$

where $R = 1.0$ and $\theta(\mathbf{x})$ is the angular polar coordinate of $\mathbf{x}$.

Domain 2 (*Square: Simply connected domain, piecewise smooth boundary*).

$$\begin{aligned} \Omega &= \{\mathbf{x} = (x_1, x_2) | -R < x_1, x_2 < R\}, \\ \Gamma &= \{\mathbf{x} = (x_1, x_2) | -R \leqslant x_1 \leqslant R, x_2 = \pm R\} \cup \{\mathbf{x} = (x_1, x_2) | x_1 = \pm R, -R \leqslant x_2 \leqslant R\}, \\ \Gamma_1 &= \{\mathbf{x} = (x_1, x_2) \in \Gamma | -R \leqslant x_1 \leqslant R, x_2 = \pm R\} \\ &\quad \cup \{\mathbf{x} = (x_1, x_2) \in \Gamma | x_1 = R, -R \leqslant x_2 \leqslant R\}, \\ \Gamma_2 &= \{\mathbf{x} = (x_1, x_2) \in \Gamma | x_1 = -R, -R < x_2 < R\}, \end{aligned} \tag{37}$$

where $R = 0.5$.

Domain 3 (*Annulus: Doubly connected domain, smooth boundary*).

$$\begin{aligned} \Omega &= \{\mathbf{x} = (x_1, x_2) | R_i^2 < x_1^2 + x_2^2 < R_o^2\}, \\ \Gamma &= \{\mathbf{x} = (x_1, x_2) | x_1^2 + x_2^2 = R_i^2\} \cup \{\mathbf{x} = (x_1, x_2) | x_1^2 + x_2^2 = R_o^2\}, \\ \Gamma_1 &= \{\mathbf{x} = (x_1, x_2) \in \Gamma | x_1^2 + x_2^2 = R_i^2\}, \\ \Gamma_2 &= \{\mathbf{x} = (x_1, x_2) \in \Gamma | x_1^2 + x_2^2 = R_o^2\}, \end{aligned} \tag{38}$$

where $R_i = 0.25$ and $R_o = 1.0$.

Domain 4 (*Square with a circular hole: Doubly connected domain, piecewise smooth boundary*).

$$\Omega = \{\mathbf{x} = (x_1, x_2) | -R_o < x_1, x_2 < R_o\} \backslash \{\mathbf{x} = (x_1, x_2) | x_1^2 + x_2^2 \leqslant R_i^2\},$$

$$\begin{aligned} \Gamma = {} & \{\mathbf{x} = (x_1, x_2) | -R_o \leqslant x_1 \leqslant R_o, x_2 = \pm R_o\} \\ & \cup \{\mathbf{x} = (x_1, x_2) | x_1 = \pm R_o, -R_o \leqslant x_2 \leqslant R_o\} \\ & \cup \{\mathbf{x} = (x_1, x_2) | x_1^2 + x_2^2 = R_i^2\}, \end{aligned}$$

$$\begin{aligned} \Gamma_1 = {} & \{\mathbf{x} = (x_1, x_2) \in \Gamma | -R_o \leqslant x_1 \leqslant R_o, x_2 = \pm R_o\} \\ & \cup \{\mathbf{x} = (x_1, x_2) \in \Gamma | x_1 = \pm R_o, -R_o \leqslant x_2 \leqslant R_o\}, \end{aligned}$$

$$\Gamma_2 = \{\mathbf{x} = (x_1, x_2) \in \Gamma | x_1^2 + x_2^2 = R_i^2\}, \tag{39}$$

where $R_i = 0.25$ and $R_o = 0.5$.

The following DRBEM discretizations are used to solve the Cauchy problem given by Eqs. (1) and (2) for examples (34) and (35) in the geometries described above:

(i) *Domain* 1: $N = 40, 60, 80$ boundary collocation points ($N_1/3 = N_2 = N/4$) and $L = 20, 40, 60$ internal collocation points, respectively, uniformly distributed on l internal circles with radii $r_n = [n/(l+1)]\,R$, $n = 1, \ldots, l$, where $l = 2, 4, 6$.
(ii) *Domain* 2: $N = 40, 60, 80$ boundary collocation points ($N_1/3 = N_2 = N/4$) and $L = 16, 36, 64$ internal collocation points, respectively, uniformly distributed on a square grid.
(iii) *Domain* 3: $N = 40, 60, 80$ boundary collocation points ($N_1 = N_2 = N/2$) and $L = 20, 30, 40$ internal collocation points, respectively, uniformly distributed on l internal circles with radii $r_n = R_i + [n/(l+1)](R_o - R_i)$, $n = 1, \ldots, l$, where $l = 2, 3, 4$.
(iv) *Domain* 4: $N = 40, 80, 160$ boundary collocation points ($N_1 = N_2 = N/2$) and $L = 16, 28, 60$ internal collocation points, respectively, uniformly distributed on a square grid excluding the hole.

5.2. Accuracy of the method

In order to investigate the accuracy of the numerical method proposed, for every regularization parameter, λ, we evaluate the root mean square (RMS) error for the acoustical field, u, and the normal velocity of the sound, ϕ, on the under-specified boundary Γ_1 defined as

$$e_u(\lambda) = \sqrt{\frac{1}{N_2} \sum_{k=N_1+1}^{N} (u_k^{(\lambda)} - u_k^{(\mathrm{an})})^2}, \quad e_\phi(\lambda) = \sqrt{\frac{1}{N_2} \sum_{k=N_1+1}^{N} (\phi_k^{(\lambda)} - \phi_k^{(\mathrm{an})})^2}, \tag{40}$$

where $u_k^{(\lambda)}$ and $\phi_k^{(\lambda)}$ are the acoustical field and the normal velocity of the sound calculated at the boundary collocation point $\mathbf{x}^k \in \Gamma_2$ using the regularization parameter λ, respectively, and $u_k^{(\mathrm{an})}$ and $\phi_k^{(\mathrm{an})}$ are the analytical values for the acoustical field and the normal velocity of the sound at the boundary collocation point $\mathbf{x}^k \in \Gamma_2$, respectively. The RMS error in predicting the acoustical field, u, inside the solution domain Ω may also be evaluated by using the expression

$$e_u^{\Omega}(\lambda) = \sqrt{\frac{1}{L} \sum_{l=1}^{L} (u_l^{(\lambda)} - u_l^{(\mathrm{an})})^2}, \tag{41}$$

where $u_l^{(\lambda)}$ and $u_l^{(\mathrm{an})}$ are the numerical and the analytical values for the acoustical field at the internal collocation point $\mathbf{x}^l \in \Omega$, respectively. However, this is not pursued here since $e_u^{\Omega}(\lambda)$ has an evolution similar to that of the RMS errors $e_u(\lambda)$ and $e_\phi(\lambda)$.

The acoustical field $u|_{\Gamma_1} = u^{(\mathrm{an})}|_{\Gamma_1}$ has been perturbed as $\tilde{u} = u + \delta u$, where δu is a Gaussian random variable with mean zero and standard deviation $\sigma = \max_{\Gamma_1}|u| \times (p_u/100)$, generated by the NAG subroutine G05DDF, and p_u% is the percentage of additive noise included in the input data $u|_{\Gamma_1}$ in order to simulate the inherent measurement errors. Figs. 1(a) and (b) show the RMS errors e_u and e_ϕ, respectively, as functions of the regularization parameter, λ, obtained for the Cauchy problem given by Example 1 in the Domain 1 using $N = 80$ boundary collocation points, $L = 60$ internal collocation points, $p_u = 1\%$ noise added into the input data $u|_{\Gamma_1}$ and various approximating functions, namely the RBFs $f(r) = 1 + r$, $f(r) = 1 + r + r^3$ and $f(r) = 1 + r + r^3 + r^5$, and the TPS $f(r) = r^2 \ln r$. It can be seen from these figures that both RMS errors e_u and e_ϕ attain the minimum for an optimal value of the regularization parameter, λ, of about $\lambda_{\mathrm{opt}} = 1.0 \times 10^{-6}$ for all the approximating functions, f, used. In addition, for all the values of the regularization parameter, λ, and the approximating functions, f, as expected, $e_u < e_\phi$, i.e. the numerical acoustical field, $u^{(\lambda)}$, is more accurate than the numerical normal velocity of the sound, $\phi^{(\lambda)}$. Although not presented here, it is reported that the same conclusions have been obtained for the Cauchy problems given by Example 1 in the Domains 2–4, as well as for Example 2 in the Domains 1–4.

With respect to the accuracy achieved, it can be seen from Figs. 1(a) and (b) that the best numerical results for the acoustical field and normal velocity of the sound in the case of Example 1 in the Domain 1 have been obtained for the RBF $f(r) = 1 + r$, followed by the RBF $f(r) = 1 + r + r^3$ and the TPS $f(r) = r^2 \ln r$, whilst the RBF $f(r) = 1 + r + r^3 + r^5$ has provided the most inaccurate numerical results. Similar conclusions have been drawn in the case of Example 1 in the Domain 2 (also a simply connected domain but with a piecewise smooth boundary). Although not presented herein, it is reported that, in the case of both examples considered in the Domains 3 and 4, i.e. doubly connected domains with smooth and piecewise smooth boundaries, respectively, from the accuracy viewpoint the TPS $f(r) = r^2 \ln r$ has provided the best numerical results for the acoustical field and normal velocity of the sound, followed by the RBFs $f(r) = 1 + r + r^3 + r^5$ and $f(r) = 1 + r$, whilst the numerical results obtained using the RBF $f(r) = 1 + r + r^3$ have been found the most inaccurate.

The analytical and numerical solutions for the acoustical field $u|_{\Gamma_2}$ and the normal velocity of the sound $\phi|_{\Gamma_2}$, obtained using the regularization parameter, λ, given by the L-curve criterion and various approximating functions, namely $f(r) = 1 + r$, $f(r) = 1 + r + r^3$, $f(r) = 1 + r + r^3 + r^5$ and $f(r) = r^2 \ln r$, for Example 1 in the Domain 1 and Example 2 in the Domain 3 are presented in Figs. 2 and 3, respectively. From these figures, it can be seen that the numerical results for the acoustical field and the normal velocity of the sound on the boundary Γ_2 are in good agreement with their analytical values for Example 1 in the Domain 1 and Example 2 in the Domain 3 when using the approximating functions $f(r) = 1 + r$ and $f(r) = r^2 \ln r$, respectively. It should be noted that the numerical method proposed in this study provides more accurate approximates for the

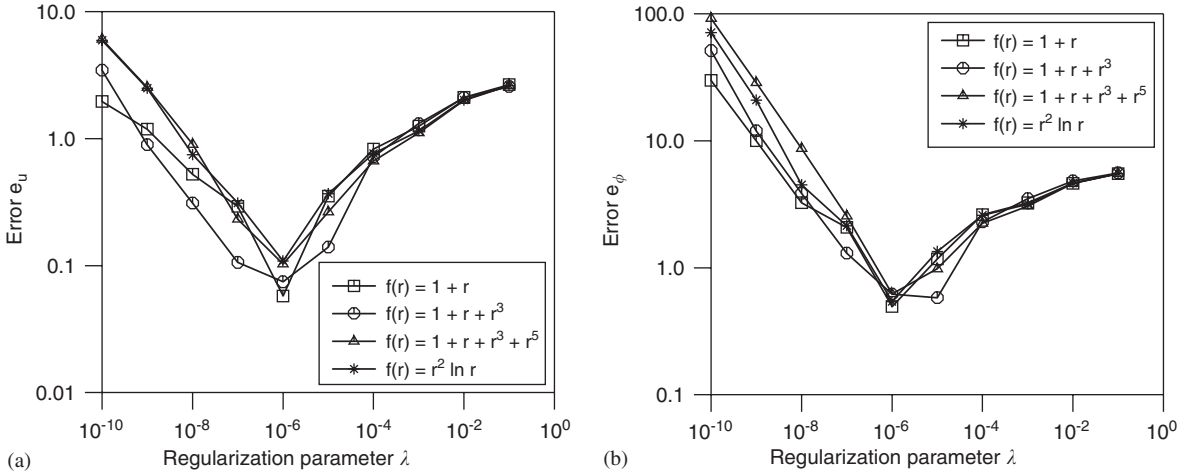

Fig. 1. The accuracy errors (a) e_u, and (b) e_ϕ as functions of the regularization parameter, λ, obtained with $N = 80$ boundary collocation points, $L = 60$ internal collocation points, $p_u = 1\%$ noise added into the input data $u|_{\Gamma_1}$ and various approximating functions, namely $f(r) = 1 + r$ $(-\square-)$, $f(r) = 1 + r + r^3$ $(-\bigcirc-)$, $f(r) = 1 + r + r^3 + r^5$ $(-\triangle-)$ and $f(r) = r^2 \ln r$ $(-*-)$, for Example 1 in the Domain 1.

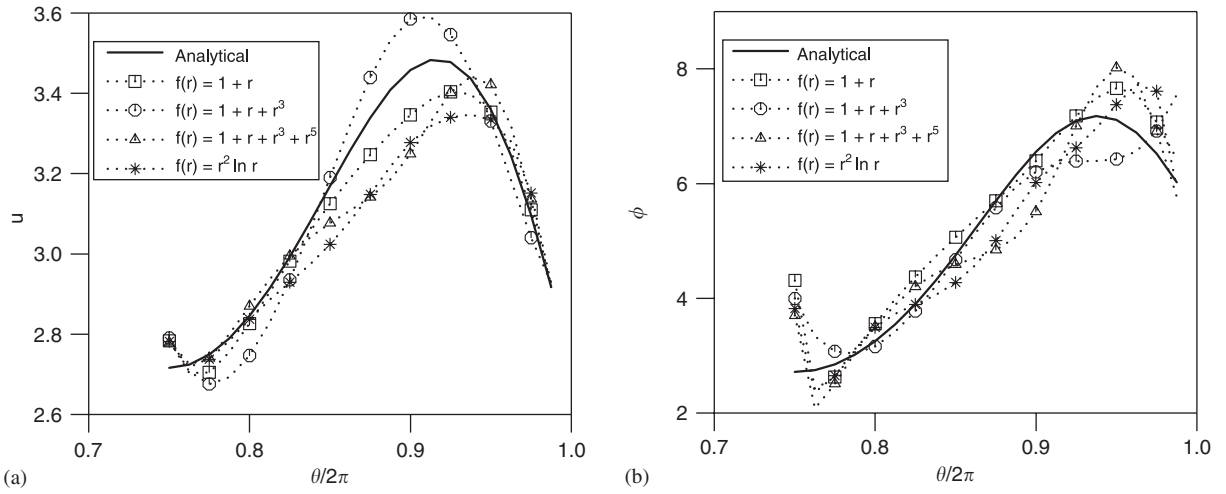

Fig. 2. (a) The analytical solution $u^{(an)}$ (—) and the numerical solution $u^{(\lambda)}$, and (b) the analytical solution $\phi^{(an)}$ (—) and the numerical solution $\phi^{(\lambda)}$, obtained with $N = 80$ boundary collocation points, $L = 40$ internal collocation points, $p_u = 1\%$ noise added into the input data $u|_{\Gamma_1}$ and various approximating functions, namely $f(r) = 1 + r$ ($\cdots\Box\cdots$), $f(r) = 1 + r + r^3$ ($\cdots\bigcirc\cdots$), $f(r) = 1 + r + r^3 + r^5$ ($\cdots\triangle\cdots$) and $f(r) = r^2 \ln r$ ($\cdots*\cdots$), for Example 1 in the Domain 1.

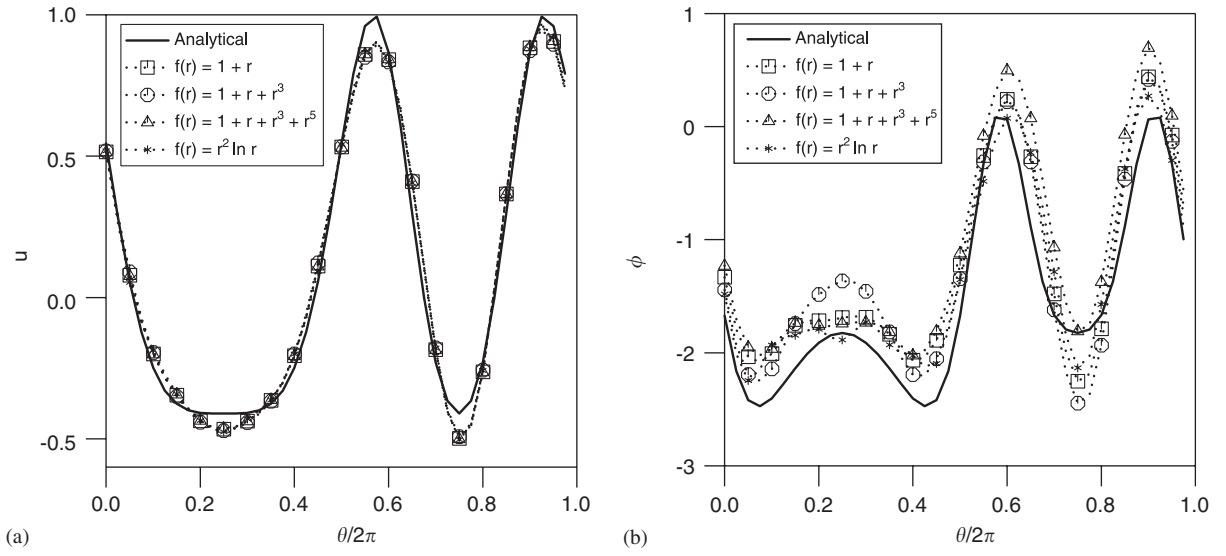

Fig. 3. (a) The analytical solution $u^{(an)}$ (—) and the numerical solution $u^{(\lambda)}$, and (b) the analytical solution $\phi^{(an)}$ (—) and the numerical solution $\phi^{(\lambda)}$, obtained with $N = 80$ boundary collocation points, $L = 40$ internal collocation points, $p_u = 1\%$ noise added into the input data $u|_{\Gamma_1}$ and various approximating functions, namely $f(r) = 1 + r$ ($\cdots\Box\cdots$), $f(r) = 1 + r + r^3$ ($\cdots\bigcirc\cdots$), $f(r) = 1 + r + r^3 + r^5$ ($\cdots\triangle\cdots$) and $f(r) = r^2 \ln r$ ($\cdots*\cdots$), for Example 2 in the Domain 3.

acoustical field and the normal velocity of the sound in the case of a doubly connected domain (Domain 3) than in the case of a simply connected domain (Domain 1). Similar results have been obtained for the Cauchy problem corresponding to Examples 1 and 2 in the Domains 2 and 4 and hence they are not presented here.

5.3. Stability of the method

In this section, we investigate the stability of the numerical method proposed in this study. To do so, we consider the Cauchy problem (1) and (2) for Example 1 in the Domain 2 and Example 2 in the Domain 4, and

various levels of noise added into the input acoustical field data on the overspecified boundary Γ_1, namely $p_u = 1, 2, 3$, for a given approximating function. More precisely, we set $f(r) = 1 + r$ and $f(r) = r^2 \ln r$ for Example 1 in the Domain 2 and Example 2 in the Domain 4, respectively.

Figs. 4(a) and (b) illustrate the behaviour of the RMS errors e_u and e_ϕ, respectively, for the Cauchy problem given by Example 1 in the Domain 2. From these figures it can be seen that both errors e_u and e_ϕ decrease with respect to decreasing the amount of noise, p_u, added into the input data $u|_{\Gamma_1}$ for all the values of the regularization parameter, λ. In addition, for a fixed value of the regularization parameter and a fixed level of noise added into the input acoustical field data, $e_u < e_\phi$. Similar results have been obtained for the Cauchy problem corresponding to Example 2 in the Domain 4 and these are shown in Figs. 5(a) and (b). Furthermore, from Figs. 4 and 5 it can be noticed that, for the all the levels of noise considered, the minimum in the RMS errors e_u and e_ϕ is attained for an optimal value of the regularization parameter of about $\lambda_{\text{opt}} = 1.0 \times 10^{-4}$ in the case of Example 1 in the Domain 2 and $\lambda_{\text{opt}} = 1.0 \times 10^{-5}$ in the case of Example 2 in the Domain 4. This optimal value for the regularization parameter is the same as that obtained by employing the L-curve criterion, i.e. by chosing the regularization parameter at the "corner" of the L-curves corresponding to Example 1 in the Domain 2 and Example 2 in the Domain 4 which are presented in Figs. 6(a) and (b), respectively.

The numerical solutions for the acoustical field and the normal velocity of the sound obtained for Example 1 in the Domain 2 and Example 2 in the Domain 4 in comparison with their corresponding analytical values are illustrated in Figs. 7 and 8, respectively. It can be seen from these figures that numerical solutions retrieved on the under-specified boundary Γ_2 using the DRBEM combined with the zeroth-order Tikhonov regularization method are stable with respect to decreasing the noise added into the input acoustical field for both examples considered. From Figs. 7(a) and (b) it can be observed that in the case of Example 1 in the Domain 2, i.e. simply connected domain with piecewise smooth boundary, the numerical results for the acoustical field are very accurate, while those obtained for the normal velocity of the sound, although they are not that accurate, they do provide a reasonable approximation to the analytical solution. However, the values for both the acoustical field and the normal velocity of the sound numerically retrieved on the boundary Γ_2 in the case of Example 2 in the Domain 4, i.e. doubly connected domain with piecewise smooth boundary, are very accurate and represent very good approximations to their analytical values. Although not presented, it is reported that similar results have been obtained for the other examples presented in this study, as well as for perturbed input normal velocity of the sound on the over-specified boundary Γ_1.

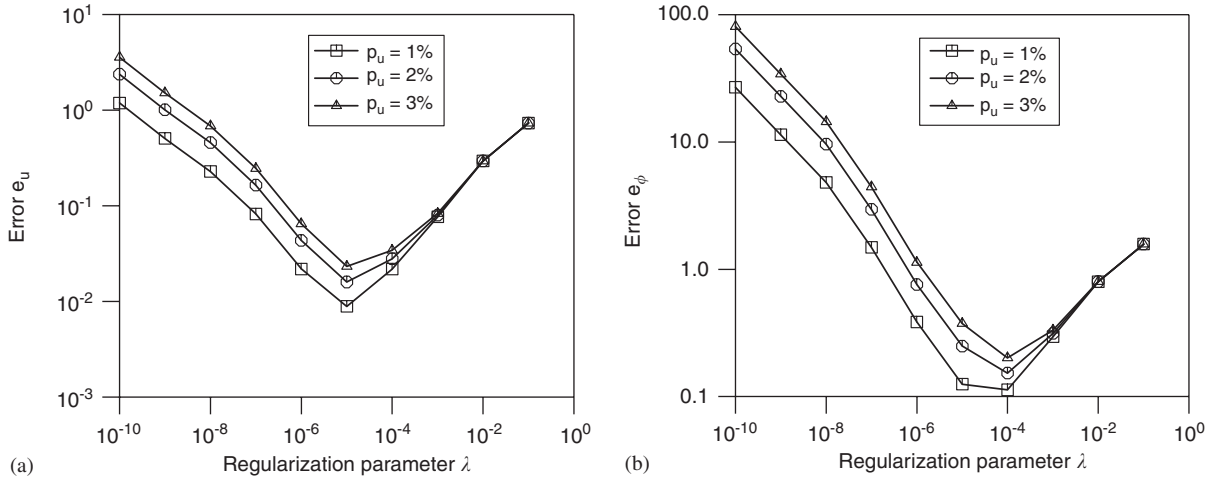

Fig. 4. The accuracy errors (a) e_u, and (b) e_ϕ as functions of the regularization parameter, λ, obtained with $N = 80$ boundary collocation points, $L = 64$ internal collocation points, the approximating function $f(r) = 1 + r$ and various levels of noise added into the input data $u|_{\Gamma_1}$, namely $p_u = 1\%$ $(-\square-)$, $p_u = 2\%$ $(-\bigcirc-)$ and $p_u = 3\%$ $(-\triangle-)$, for Example 1 in the Domain 2.

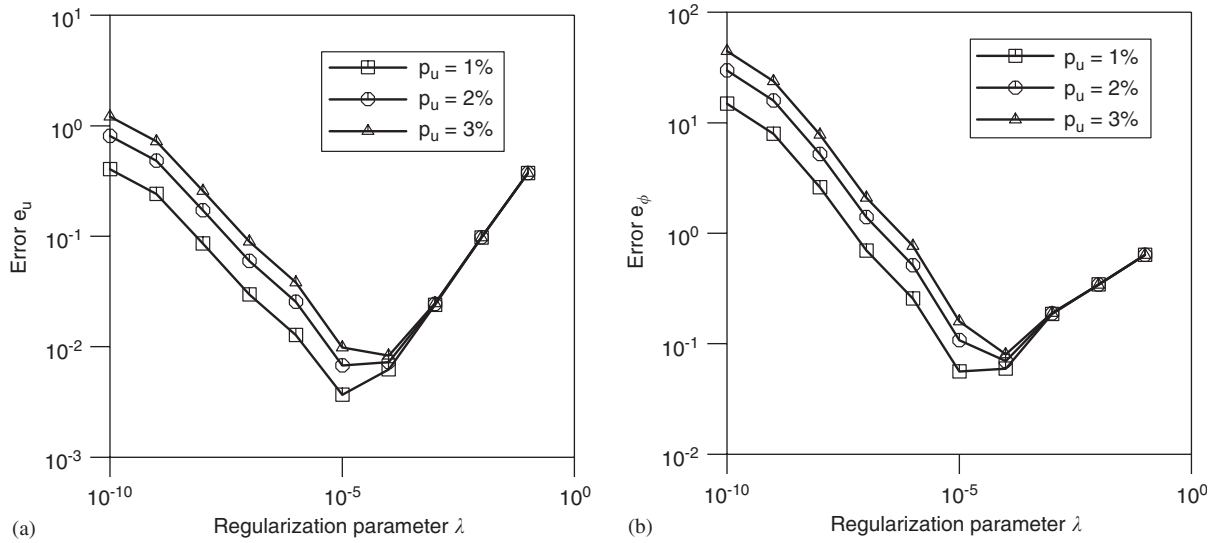

Fig. 5. The accuracy errors (a) e_u, and (b) e_ϕ as functions of the regularization parameter, λ, obtained with $N = 80$ boundary collocation points, $L = 28$ internal collocation points, the approximating function $f(r) = r^2 \ln r$ and various levels of noise added into the input data $u|_{\Gamma_1}$, namely $p_u = 1\%$ $(-\square-)$, $p_u = 2\%$ $(-\bigcirc-)$ and $p_u = 3\%$ $(-\triangle-)$, for Example 2 in the Domain 4.

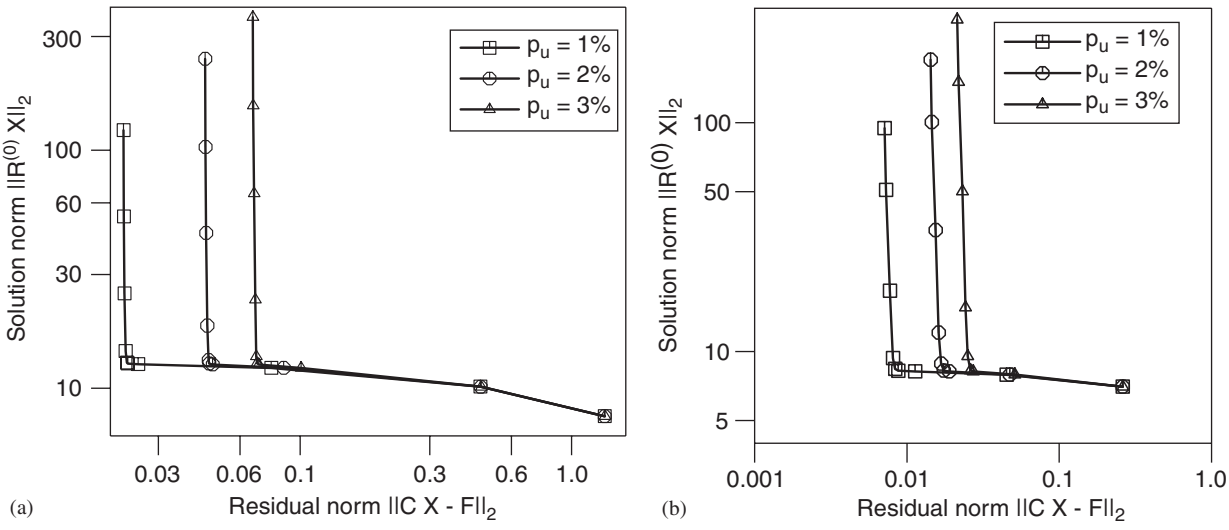

Fig. 6. (a) The L-curves obtained with $N = 80$ boundary collocation points, $L = 64$ internal collocation points, the approximating function $f(r) = 1 + r$ and various levels of noise added into the input data $u|_{\Gamma_1}$, namely $p_u = 1\%$ $(-\square-)$, $p_u = 2\%$ $(-\bigcirc-)$ and $p_u = 3\%$ $(-\triangle-)$, for Example 1 in the Domain 2. (b) The L-curves obtained with $N = 80$ boundary collocation points, $L = 28$ internal collocation points, the approximating function $f(r) = r^2 \ln r$ and various levels of noise added into the input data $u|_{\Gamma_1}$, namely $p_u = 1\%$ $(-\square-)$, $p_u = 2\%$ $(-\bigcirc-)$ and $p_u = 3\%$ $(-\triangle-)$, for Example 2 in the Domain 4.

5.4. Convergence of the method

The convergence of the numerical method described in this paper is analysed by considering the Cauchy problems given by Example 1 in the Domains 3 and 4, and various DRBEM discretizations for a given approximating function and a given level of noise added into the input data. More precisely, we set $f(r) = r^2 \ln r$ and $p_u = 1\%$, and consider $N = 40, 60, 80$ boundary collocation points $(N_1 = N_2 = N/2)$ and $L = 20, 30, 40$ internal collocation points uniformly distributed on l internal circles with radii

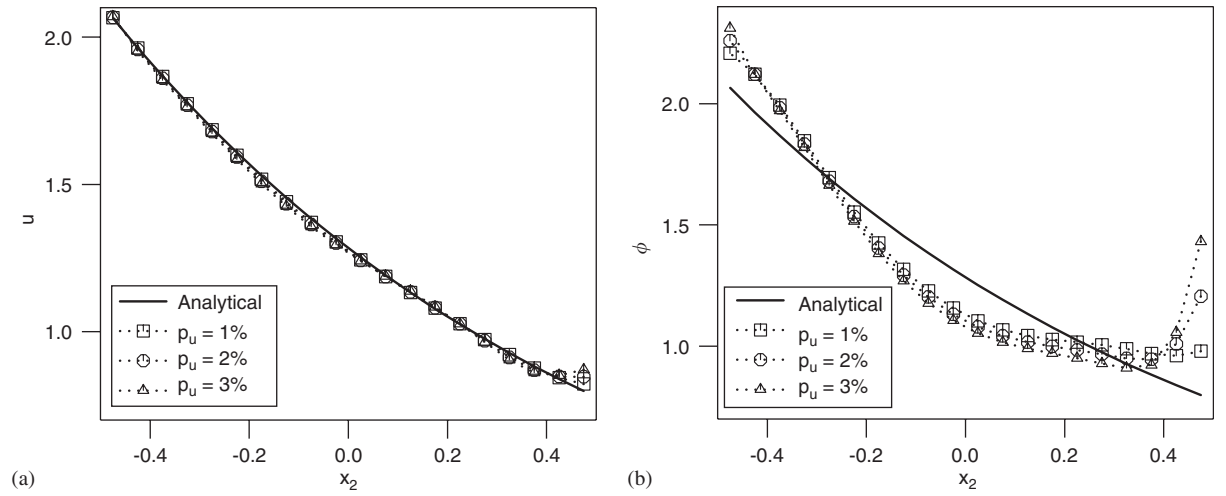

Fig. 7. (a) The analytical solution $u^{(\mathrm{an})}$ (—) and the numerical solution $u^{(\lambda)}$, and (b) the analytical solution $\phi^{(\mathrm{an})}$ (—) and the numerical solution $\phi^{(\lambda)}$, obtained with $N = 80$ boundary collocation points, $L = 60$ internal collocation points, $\lambda = \lambda_{\mathrm{opt}}$, the approximating function $f(r) = 1 + r$ and various levels of noise added into the input data $u|_{\Gamma_1}$, namely $p_u = 1\%$ ($\cdots\square\cdots$), $p_u = 2\%$ ($\cdots\bigcirc\cdots$) and $p_u = 3\%$ ($\cdots\triangle\cdots$), for Example 1 in the Domain 2.

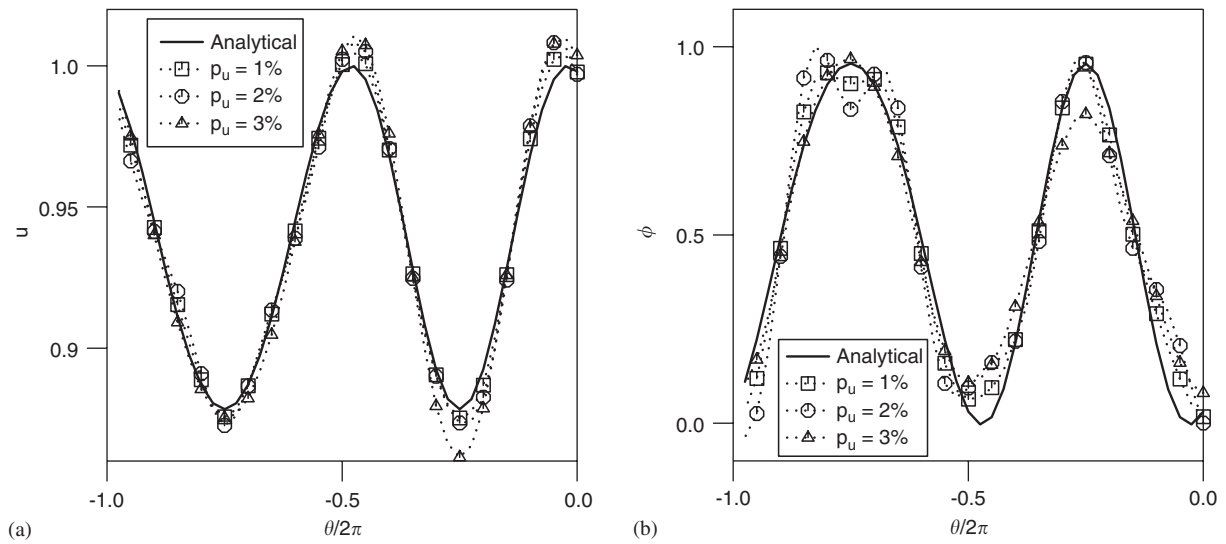

Fig. 8. (a) The analytical solution $u^{(\mathrm{an})}$ (—) and the numerical solution $u^{(\lambda)}$, and (b) the analytical solution $\phi^{(\mathrm{an})}$ (—) and the numerical solution $\phi^{(\lambda)}$, obtained with $N = 80$ boundary collocation points, $L = 60$ internal collocation points, $\lambda = \lambda_{\mathrm{opt}}$, the approximating function $f(r) = r^2 \ln r$ and various levels of noise added into the input data $u|_{\Gamma_1}$, namely $p_u = 1\%$ ($\cdots\square\cdots$), $p_u = 2\%$ ($\cdots\bigcirc\cdots$) and $p_u = 3\%$ ($\cdots\triangle\cdots$), for Example 2 in the Domain 4.

$r_n = R_i + [n/(l+1)](R_o - R_i)$, $n = 1, \ldots, l$, where $l = 2, 3, 4$, and $N = 40, 80, 160$ boundary collocation points ($N_1 = N_2 = N/2$) and $L = 16, 28, 60$ internal collocation points uniformly distributed on a square grid excluding the hole for Example 1 in the Domains 3 and 4, respectively.

Figs. 9(a) and (b) show the RMS error e_u defined by relation (40) as a function of the regularization parameter, λ, obtained using the aforementioned DRBEM discretizations for the Cauchy problems given by Example 1 in the Domains 3 and 4, respectively. It can be seen from these figures that the RMS error e_u attains the minimum for an optimal value of the regularization parameter, λ, of about $\lambda_{\mathrm{opt}} = 1.0 \times 10^{-5}$ in the case of Example 1 in the Domain 3 and $\lambda_{\mathrm{opt}} = 1.0 \times 10^{-4}$ in the case of Example 1 in the Domain 4 for all the

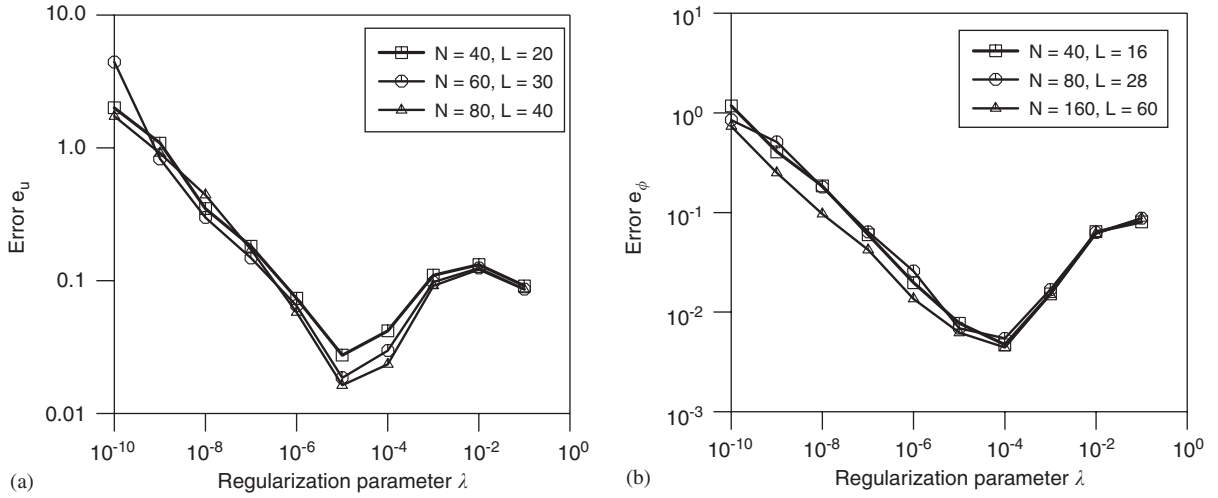

Fig. 9. (a) The accuracy error e_u as a function of the regularization parameter, λ, obtained with $p_u = 1\%$ noise added into the input data $u|_{\Gamma_1}$, the approximating function $f(r) = r^2 \ln r$ and various DRBEM discretizations, namely $N = 40$ and $L = 20$ ($-\square-$), $N = 60$ and $L = 30$ ($-\bigcirc-$), and $N = 80$ and $L = 40$ ($-\triangle-$), for Example 1 in the Domain 3. (b) The accuracy error e_u as a function of the regularization parameter, λ, obtained with $p_u = 1\%$ noise added into the input data $u|_{\Gamma_1}$, the approximating function $f(r) = r^2 \ln r$ and various DRBEM discretizations, namely $N = 40$ and $L = 16$ ($-\square-$), $N = 80$ and $L = 28$ ($-\bigcirc-$), and $N = 160$ and $L = 60$ ($-\triangle-$), for Example 1 in the Domain 4.

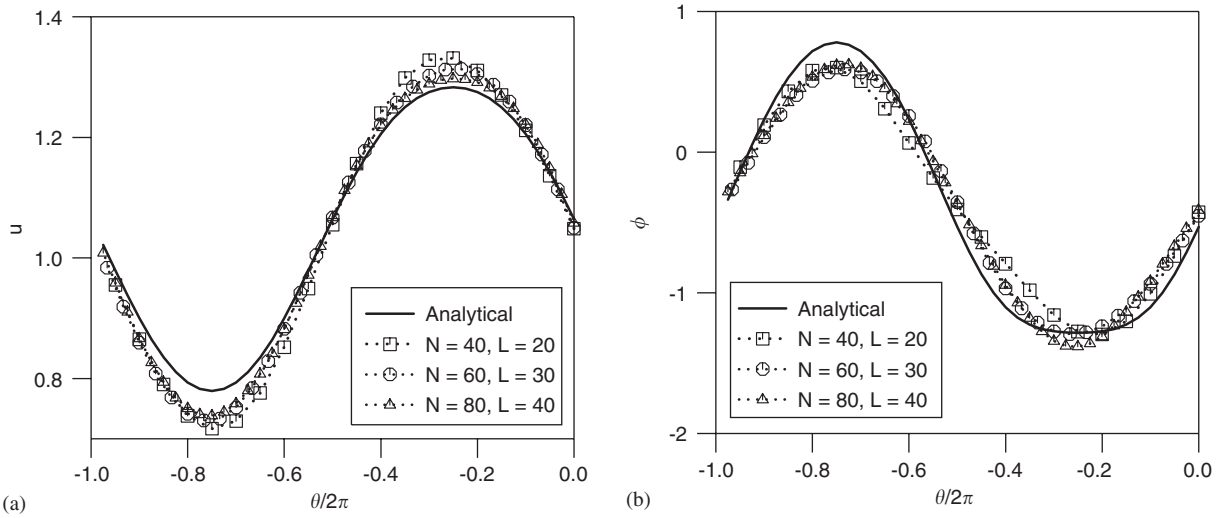

Fig. 10. (a) The analytical solution $u^{(an)}$ (—) and the numerical solution $u^{(\lambda)}$, and (b) the analytical solution $\phi^{(an)}$ (—) and the numerical solution $\phi^{(\lambda)}$, obtained with $p_u = 1\%$ noise added into the input data $u|_{\Gamma_1}$, the approximating function $f(r) = r^2 \ln r$ and various DRBEM discretizations, namely $N = 40$ and $L = 20$ ($\cdots\square\cdots$), $N = 60$ and $L = 30$ ($\cdots\bigcirc\cdots$), and $N = 80$ and $L = 40$ ($\cdots\triangle\cdots$), for Example 1 in the Domain 3.

DRBEM meshes considered. Moreover, for all the values of the regularization parameter, λ, the RMS error e_u decreases with respect to refining the DRBEM mesh. Although not presented here, it is reported that the RMS error e_ϕ corresponding to Example 1 in the Domains 3 and 4 has a similar behaviour.

The analytical and the numerical results for the acoustical field $u|_{\Gamma_2}$ and the normal velocity of the sound $\phi|_{\Gamma_2}$, retrieved using the regularization parameter, λ, given by the L-curve criterion, the approximating function $f(r) = r^2 \ln r$, $p_u = 1\%$, and $N = 40, 60, 80$ boundary collocation points and $L = 20, 30, 40$ internal collocation points are illustrated in Figs. 10(a) and (b), respectively. From these figures, it can be seen that the numerical solutions for both the acoustical field and the normal velocity of the sound on the under-specified

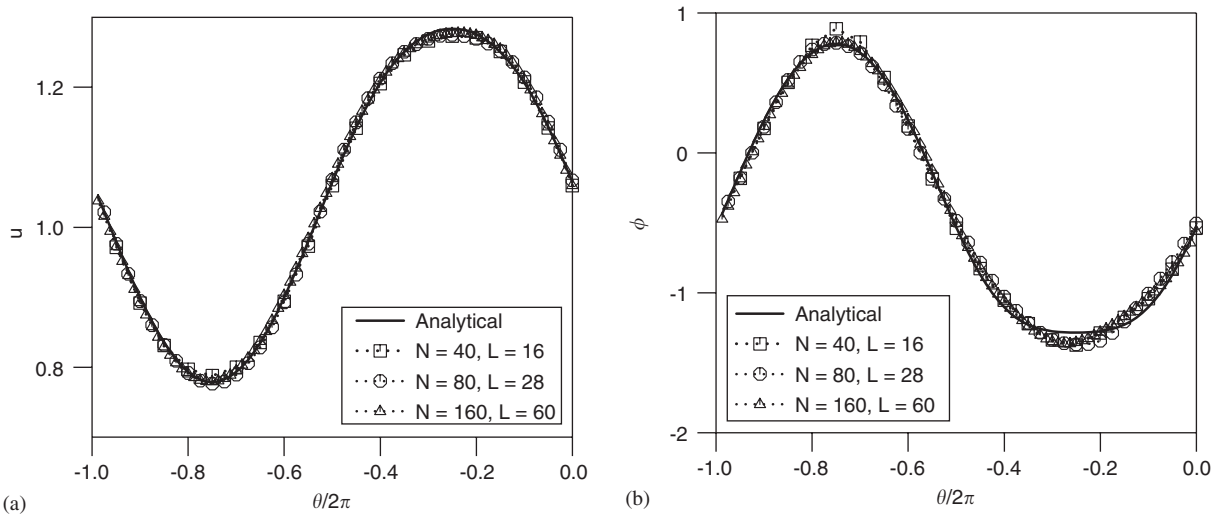

Fig. 11. (a) The analytical solution $u^{(an)}$ (—) and the numerical solution $u^{(\lambda)}$, and (b) the analytical solution $\phi^{(an)}$ (—) and the numerical solution $\phi^{(\lambda)}$, obtained with $p_u = 1\%$ noise added into the input data $u|_{\Gamma_1}$, the approximating function $f(r) = r^2 \ln r$ and various DRBEM discretizations, namely $N = 40$ and $L = 16$ ($\cdots \square \cdots$), $N = 80$ and $L = 28$ ($\cdots \bigcirc \cdots$), and $N = 160$ and $L = 60$ ($\cdots \triangle \cdots$), for Example 1 in the Domain 4.

boundary Γ_2 converge towards their corresponding analytical solutions with respect to increasing the number of boundary and internal DRBEM collocation points. A similar conclusion can be drawn from Figs. 11(a) and (b) which present the numerical solutions for the acoustical field and the normal velocity of the sound obtained using various DRBEM meshes in comparison to their analytical values corresponding to Example 1 in the Domain 1.

From the numerical results presented in this section, it can be concluded that the L-curve criterion has a regularizing effect and the numerical solution obtained by DRBEM-Tikhonov regularization method described in this paper is convergent and stable with respect to decreasing the level of noise added into the input data and increasing the number of DRBEM collocation points, respectively.

6. Conclusions

In this paper, we have investigated the Cauchy problem for Helmholtz-type equations with variable coefficients in the two-dimensional case. In order to deal with the instabilities of the solution of this ill-posed problem, a numerical technique based on the DRBEM combined with the zeroth-order Tikhonov regularization method has been proposed. The resulting DRBEM system of linear algebraic equations which is ill-conditioned was regularized by choosing the optimal regularization parameter according to the L-curve criterion. The proposed numerical method has been analysed in terms of accuracy, convergence and stability for four examples corresponding to the Cauchy problem in simply and doubly connected domains with both smooth and piecewise smooth boundaries. The numerical results obtained for various DRBEM discretizations, various amounts of noise added to the input data and various approximating functions showed that the method produces an accurate, convergent and stable numerical solution with respect to increasing the number of boundary and internal DRBEM collocation points and decreasing the amount of noise. It was found that the numerical solutions for the acoustical field and the normal velocity of the sound in the case of simply connected domains with smooth and piecewise smooth boundaries, e.g. disk and square, are more sensitive to the perturbed input data than the corresponding numerical solutions obtained in the case of doubly connected domains with smooth and piecewise smooth boundaries, e.g. annulus and square with a circular hole. Also, the numerical solutions retrieved for noisy input data using the DRBEM and the zeroth-order Tikhonov regularization method depend on the geometry of the solution domain, as well as on the type of approximating function employed in the DRBEM.

Acknowledgements

The authors would like to acknowledge the financial support received from the EPSRC.

References

[1] D.E. Beskos, Boundary element method in dynamic analysis: Part II (1986–1996), *ASME Applied Mechanics Review* 50 (1997) 149–197.
[2] J.T. Chen, F.C. Wong, Dual formulation of multiple reciprocity method for the acoustic mode of a cavity with a thin partition, *Journal of Sound and Vibration* 217 (1998) 75–95.
[3] I. Harari, P.E. Barbone, M. Slavutin, R. Shalom, Boundary infinite elements for the Helmholtz equation in exterior domains, *International Journal for Numerical Methods in Engineering* 41 (1998) 1105–1131.
[4] W.S. Hall, X.Q. Mao, A boundary element investigation of irregular frequencies in electromagnetic scattering, *Engineering Analysis with Boundary Elements* 16 (1995) 245–252.
[5] A.D. Kraus, A. Aziz, J. Welty, *Extended Surface Heat Transfer*, McGraw-Hill, New York, 2001.
[6] M. Manzoor, D.B. Ingham, P.J. Heggs, The one-dimensional analysis of fin assembly heat transfer, *ASME Journal of Heat Transfer* 105 (1983) 646–651.
[7] A.S. Wood, G.E. Tupholme, M.I.H. Bhatti, P.J. Heggs, Steady-state heat transfer through extended plane surfaces, *International Communications in Heat and Mass Transfer* 22 (1995) 99–109.
[8] Y. Niwa, S. Kobayashi, M. Kitahara, Determination of eigenvalues by boundary element method, in: P.K. Banerjee, R. Shaw (Eds.), *Development in Boundary Element Methods*, Applied Science Publishers, New York, 1982 (Chapter 7) pp. 143–176.
[9] A.J. Nowak, C.A. Brebbia, Solving Helmholtz equation by boundary elements using multiple reciprocity method, in: C.M. Calomagno, C.A. Brebbia (Eds.), *Computer Experiment in Fluid Flow*, CMP/Springer, Berlin, 1989, pp. 265–270.
[10] J.P. Agnantiaris, D. Polyzer, D. Beskos, Three-dimensional structural vibration analysis by the dual reciprocity BEM, *Computational Mechanics* 21 (1998) 372–381.
[11] G. Chen, J. Zhou, *Boundary Element Methods*, Academic Press, London, 1992.
[12] J. Hadamard, *Lectures on Cauchy Problem in Linear Partial Differential Equations*, University Press, London, 1923.
[13] M.R. Bai, Application of BEM-based acoustic holography to radiation analysis of sound sources with arbitrarily shaped geometries, *Journal of the Acoustical Society of America* 92 (1992) 533–549.
[14] B.K. Kim, J.G. Ih, On the reconstruction of the vibro-acoustic field over the surface enclosing an interior space using the boundary element method, *Journal of the Acoustical Society of America* 100 (1996) 3003–3016.
[15] Z. Wang, S.R. Wu, Helmholtz equation-least-squares method for reconstructing the acoustic pressure field, *Journal of the Acoustical Society of America* 102 (1997) 2020–2032.
[16] S.R. Wu, J. Yu, Application of BEM-based acoustic holography to radiation analysis of sound sources with arbitrarily shaped geometries, *Journal of the Acoustical Society of America* 104 (1998) 2054–2060.
[17] T. DeLillo, V. Isakov, N. Valdivia, L. Wang, The detection of the source of acoustical noise in two dimensions, *SIAM Journal on Applied Mathematics* 61 (2001) 2104–2121.
[18] T. DeLillo, V. Isakov, N. Valdivia, L. Wang, The detection of surface vibrations from interior acoustical pressure, *Inverse Problems* 19 (2003) 507–524.
[19] L. Marin, L. Elliott, P.J. Heggs, D.B. Ingham, D. Lesnic, X. Wen, An alternating iterative algorithm for the Cauchy problem associated to the Helmholtz equation, *Computer Methods in Applied Mechanics and Engineering* 192 (2003) 709–722.
[20] L. Marin, L. Elliott, P.J. Heggs, D.B. Ingham, D. Lesnic, X. Wen, Conjugate gradient-boundary element solution to the Cauchy problem for Helmholtz-type equations, *Computational Mechanics* 31 (2003) 367–377.
[21] L. Marin, L. Elliott, P.J. Heggs, D.B. Ingham, D. Lesnic, X. Wen, Comparison of regularization methods for solving the Cauchy problem associated with the Helmholtz equation, *International Journal for Numerical Methods in Engineering* 60 (2004) 1933–1947.
[22] L. Marin, L. Elliott, P.J. Heggs, D.B. Ingham, D. Lesnic, X. Wen, BEM solution for the Cauchy problem associated with Helmholtz-type equations by the Landweber method, *Engineering Analysis with Boundary Elements* 28 (2004) 1025–1034.
[23] P.C. Hansen, *Rank-Deficient and Discrete Ill-Posed Problems: Numerical Aspects of Linear Inversion*, SIAM, Philadelphia, 1998.
[24] D. Nardini, C.A. Brebbia, A new approach to free vibration analysis using boundary elements, in: C.A. Brebbia (Ed.), *Boundary Element Method in Engineering*, Springer, Berlin, 1982, pp. 312–326.
[25] P.W. Partridge, C.A. Brebbia, L.C. Wrobel, *The Dual Reciprocity Boundary Element Method*, CMP/Elsevier, London, 1992.
[26] A.N. Tikhonov, V.Y. Arsenin, *Methods for Solving Ill-Posed Problems*, Nauka, Moscow, 1986.
[27] P.C. Hansen, The L-curve and its use in the numerical treatment of inverse problems, in: P. Johnston (Ed.), *Computational Inverse Problems in Electrocardiology*, WIT Press, Southampton, 2001, pp. 119–142.
[28] D.L. Phillips, A technique for the numerical solution of certain integral equations of the first kind, *Journal of the Association for Computing Machinery* 9 (1962) 84–97.
[29] A.N. Tikhonov, A.S. Leonov, A.G. Yagola, *Nonlinear Ill-Posed Problems*, Chapman & Hall, London, 1998.
[30] M. Hanke, Limitations of the L-curve method in ill-posed problems, *BIT* 36 (1996) 287–301.
[31] C.R. Vogel, Non-convergence of the L-curve regularization parameter selection method, *Inverse Problems* 12 (1996) 535–547.